PETROGRAPHIC AND MINERALOGICAL CHARACTERIZATION OF GRANITOIDS AND PEGMATITES IN THE PAN-AFRICAN HARAZE DJOMBO MASSIF (BATHA, CENTRAL CHAD).

ABSTRACT

The Batha Massif, located in central Chad, occupies a key position at the transition between the Saharan Metacraton and the Pan-African Central African Fold Belt. The geodynamic evolution and metallogenic potential of this area remain poorly understood due to the scarcity of modern petrographic and mineralogical data. This study is based on a combined approach involving field surveys in the Djombo and Gleb sectors (Haraze Djombo department), optical microscopy for petrographic characterization, and high-resolution powder X-ray diffraction (XRD) for mineralogical analysis. The observations highlight two main facies: a peraluminous biotite-muscovite granite (Djombo) and a strongly altered amphibole-biotite granite (Gleb). XRD analysis of the Djombo granite reveals an assemblage dominated by quartz, microcline, albite, biotite, and tremolite. The Gleb pegmatite sample displays a monophasic signature of extremely pure and highly crystalline quartz, associated with a cataclastic texture. These data evidence post-collisional felsic magmatism emplaced during a period of crustal relaxation (~570-560 Ma). The massive quartz veins reflect an intense circulation of late- to post-orogenic hydrothermal fluids, controlled by shear zones, thereby confirming the strong metallogenic (particularly gold) potential of the area.

Keywords: Chad, Batha Massif, Pan-African, Post-collisional granite, XRD, Hydrothermalism, Gold potential.

1. INTRODUCTION

In Chad, the Precambrian basement outcrops in the Tibesti (North), Ouaddaï (East), Guéra (Central), Yadé, and Mayo-Kebbi (West) massifs, the latter belonging to the Pan-African Central African Fold Belt (Fig. 1a). These formations cover 15-20% of the territory, while the rest consists of Phanerozoic sedimentary covers. Most studies (Abdelsalam et al., 2002; Liégeois et al., 2013; Shellnutt et al., 2017) locate these regions within the Saharan Metacraton, a vast continental area of 5,000,000 km² extending from the Arabian-Nubian Shield to the Tuareg Shield, and from the Mediterranean to the Congo Craton (Fig. 1b). The Guéra Massif, in the center of the country, mainly consists of heterogeneous Ediacaran granitoids (570-560 Ma) interpreted as post-collisional, emplaced during the crustal relaxation that followed the collision between the Saharan Metacraton and the Congo Craton (610-590

Ma). Inherited zircons (~1.0 Ga and ~1.9 Ga) attest to the contribution of an ancient basement (Shellnutt et al., 2017, 2020; Blades et al., 2021). However, previous studies, mostly limited to petrographic descriptions (Vincent, 1956; Kasser, 1995), have not constrained the geodynamic evolution nor the origin of the mineralized occurrences (gold, graphite, iron) identified in the region. This study aims to characterize the mineralized granites and pegmatites of the Djombo and Gleb mountains (Haraze Djombo department, Batha region) through a petrographic and mineralogical (XRD) approach in order to: (i) define their mineralogical assemblage and emplacement context; (ii) constrain the applicable geodynamic model; (iii) assess the regional metallogenic potential.

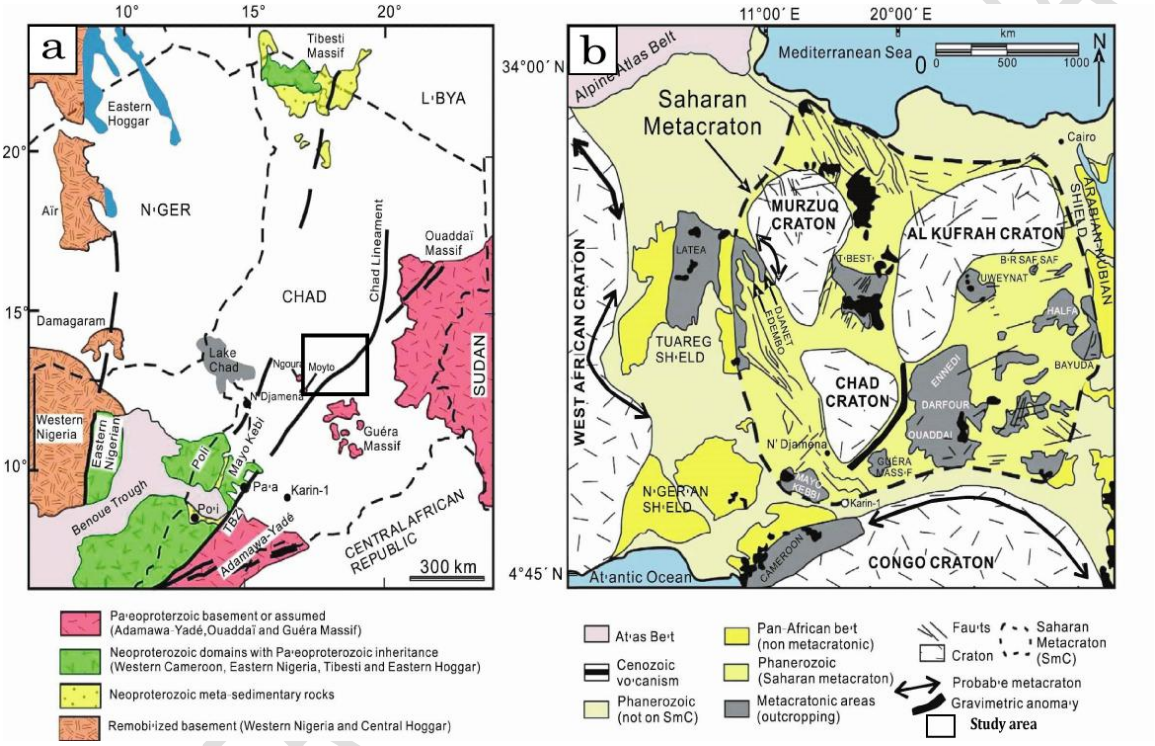

Figure 1.*The different geological correlations of the southern boundary of the Saharan Metacraton. (a) Correlation of rock units in Central Africa as interpreted by Penaye et al. (2006). (b) Boundary of the Saharan Metacraton as delineated by Abdelsalam et al. (2002) and Liégeois et al. (2013).*

2. MATERIALS AND METHODS

2.1. Sampling and Fieldwork

Sampling was conducted in the Haraze Djombo department, specifically at Mount Djombo and Mount Gleb. The equipment used included: a compass, GPS, geological hammer, and topographic maps. Representative facies and mineralized zones were identified, described, and photographed in situ.

2.2. Petrography

Selected samples were prepared as polished thin sections (standard thickness of 30 µm). Observation of textures and mineralogical assemblages was carried out at the Geology Laboratory of Babeș-Bolyai University (Cluj-Napoca, Romania) using a Nikon Optiphot T2-Pol polarizing microscope under plane-polarized light (PPL) and cross-polarized light (XPL).

2.3. X-Ray Diffraction (XRD)

Mineralogical XRD analysis was performed on powder samples at the Department of Geology, Babeș-Bolyai University (Romania). Samples were finely ground (<10 µm) using an agate mortar and then analyzed using a Bruker D8 Advance diffractometer equipped with a Cu Kα source (λ = 1.54060 Å), an Fe filter (0.01 mm), and a one-dimensional LynxEye detector. Operating parameters were: 40 kV, 40 mA, scanning from 5° to 65° (2θ) with a step size of 0.02° and a counting time of 0.2 s/step. Identification of mineral phases was performed using Diffrac.Suite EVA software and the PDF2 database (version 2.1202) from the ICDD (International Centre for Diffraction Data).

3. RESULTS

3.1. Lithology and Petrography

Mounts Djombo and Gleb, located approximately 8 km apart (Fig. 2a-b), form prominent granitic reliefs dominating a vast alluvial plain. This area is currently the focus of intense gold prospecting activities due to the presence of mineralized structures. The rock outcrops mainly expose pink granites with a granular texture, partially masked by an aeolian sand cover.

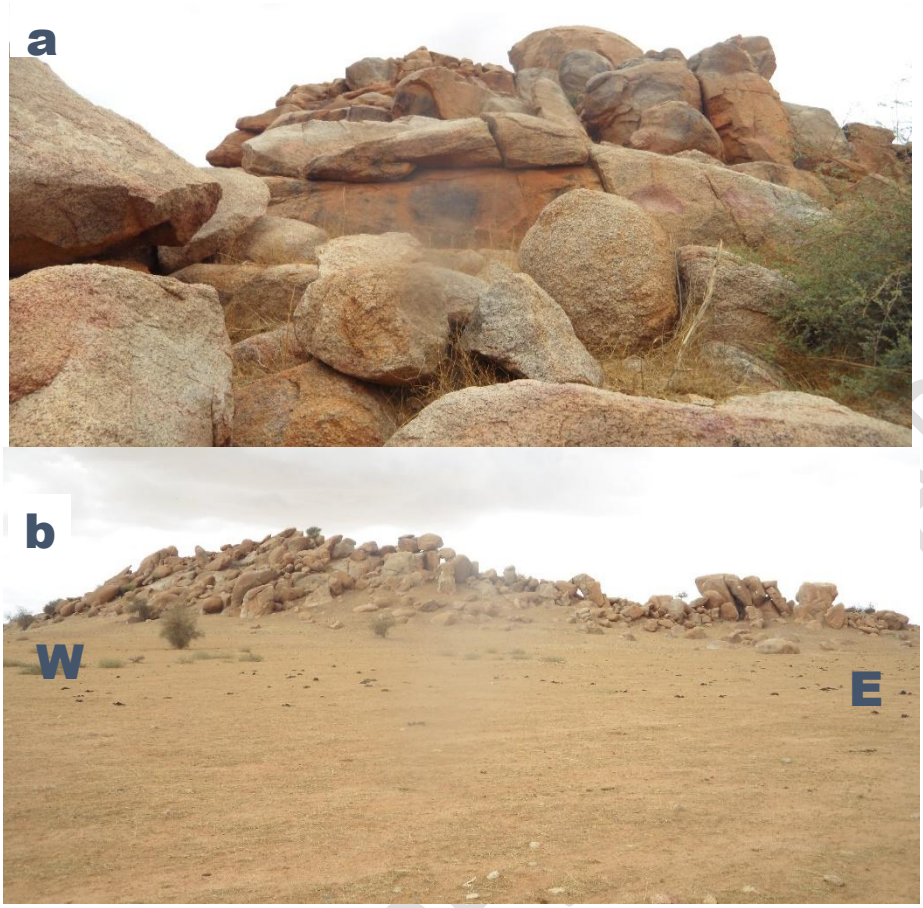

Figure 2.*Macroscopic facies of Mounts Gleb and Djombo. a-b: Outcrop and boulders on Mounts Gleb and Djombo.*

3.1.1. Amphibole-biotite granite (Mount Gleb)

The amphibole-biotite granite is medium-grained, slightly darker, and distinguished by an increased abundance of biotite and a reduced presence of K-feldspar. On a fresh fracture, the rock displays a whitish color speckled with black, with visible minerals being biotite, feldspar, and quartz (Fig. 3a). Under the microscope, this granite shows a heterogranular texture affected by intense saussuritization of plagioclases (a felted mass of sericite and clays masking the twins) and microfracturing of quartz (Fig. 3b). The mafic minerals cluster into synneusis aggregates, associating prismatic green hornblende and chloritized yellow-brown biotite (Fig. 3c). Euhedral allanite (up to 0.45 mm) is exceptionally abundant, accompanied by apatite, zircon, granular epidote, and secondary calcite (Fig. 3d).

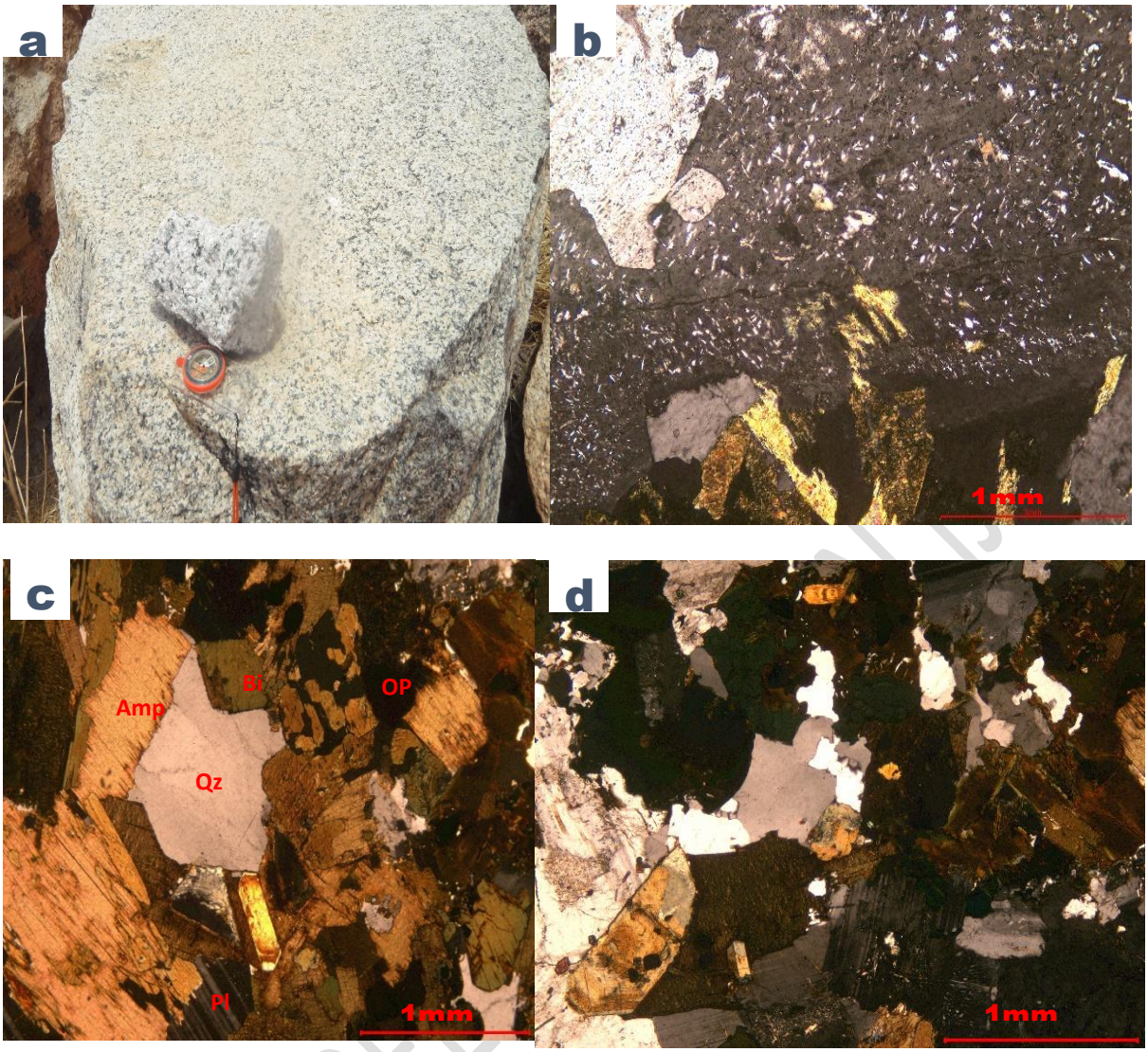

Figure 3.*Amphibole-biotite granite of Mount Gleb. a: Outcrop of altered pink boulders. b: Granular texture with saussuritized plagioclases (XPL). c: Mafic hornblende-biotite aggregate (PPL). d: Allanite, apatite, and zircon crystals (PPL).*

3.1.2. Biotite-muscovite granite (Mount Djombo)

The biotite granites outcrop as chaotic boulders on Mount Djombo and display a granular texture on fresh fractures (Fig. 4a-b). Microscopically, it exhibits a granular to slightly porphyritic texture (Fig. 4c). Subhedral plagioclase (1.4 mm) and enclosing microcline are molded by large quartz patches with undulose extinction (Fig. 4d). The petrographic particularity of this facies lies in the association of large chloritized brown biotite laths (rich in metamict zircons) with primary muscovite in clear flakes, indicating a differentiated peraluminous magmatism. Zoned prismatic allanite (up to 1.4 mm), yellow-brown titanite, and magnetite constitute the accessory assemblage (Fig. 4e).

103

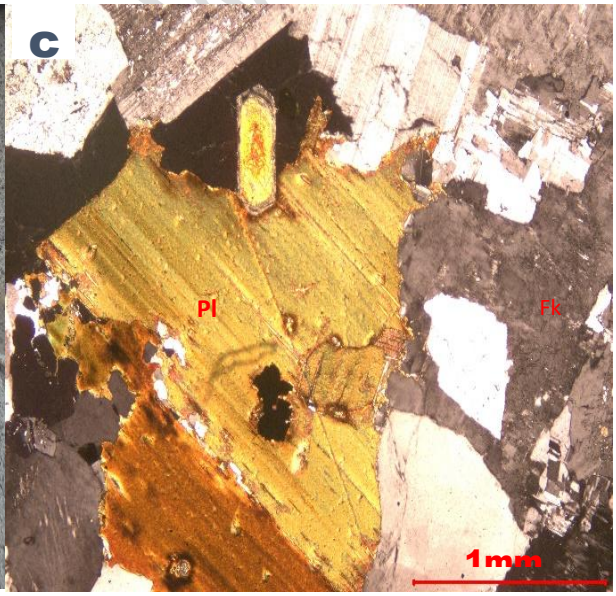

104

e

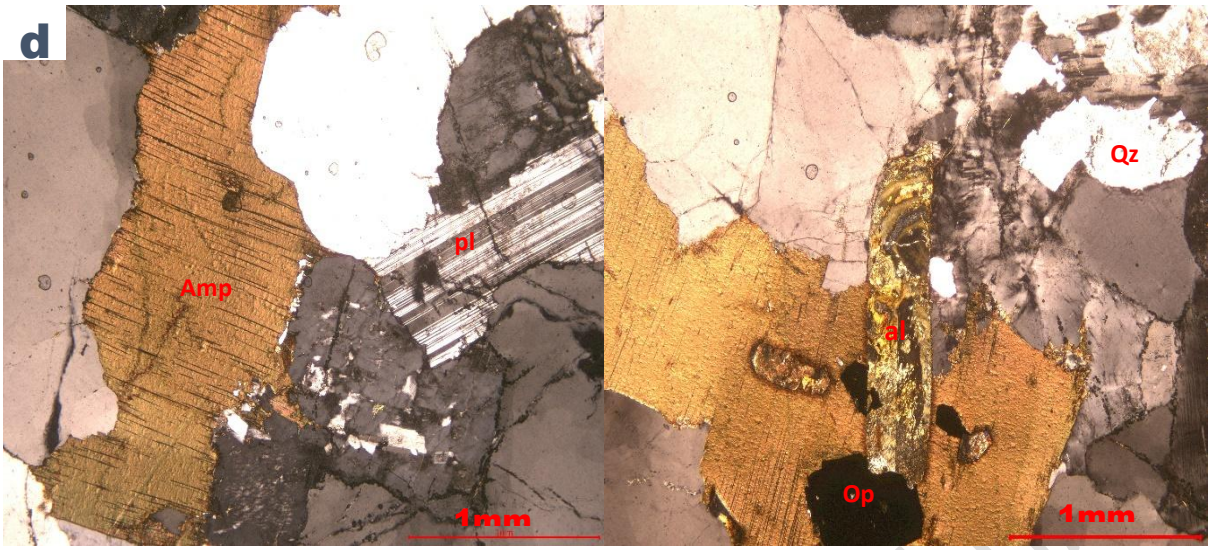

Figure 4. *Biotite-muscovite granite of Djombo (sample DJ). a-b: Fresh fracture with granular texture. c: Porphyritic granular texture (XPL). d: Plagioclase, microcline, and quartz with undulose extinction (XPL). e: Primary biotite-muscovite association and accessory minerals: zoned allanite, titanite, magnetite (XPL/PPL).*

3.1.3. Pegmatites and quartz veins (Gleb Sector)

Pegmatites and massive milky quartz veins appear frequently at the top of the mounts and in drill cores, intimately linked to gold mineralization (Fig. 5a-b). The pegmatites are often more or less altered on the surface and at depth in gold exploration drill holes, associated with quartz crystals (Fig. 5c-d). The contacts between the granites and the host rocks are quite sharp. Microscopic examination of the pegmatite reveals a spectacular cataclastic texture (Fig. 5e). Large, sharp-edged angular porphyroclasts of quartz and feldspar (up to 3.3 mm) are dispersed in a finely comminuted dark matrix. The dense network of anastomosing microfissures fragmenting the crystals is highlighted by iron oxide deposits and hydrothermal cements, indicating major brittle fracturing (Fig. 5f).

120

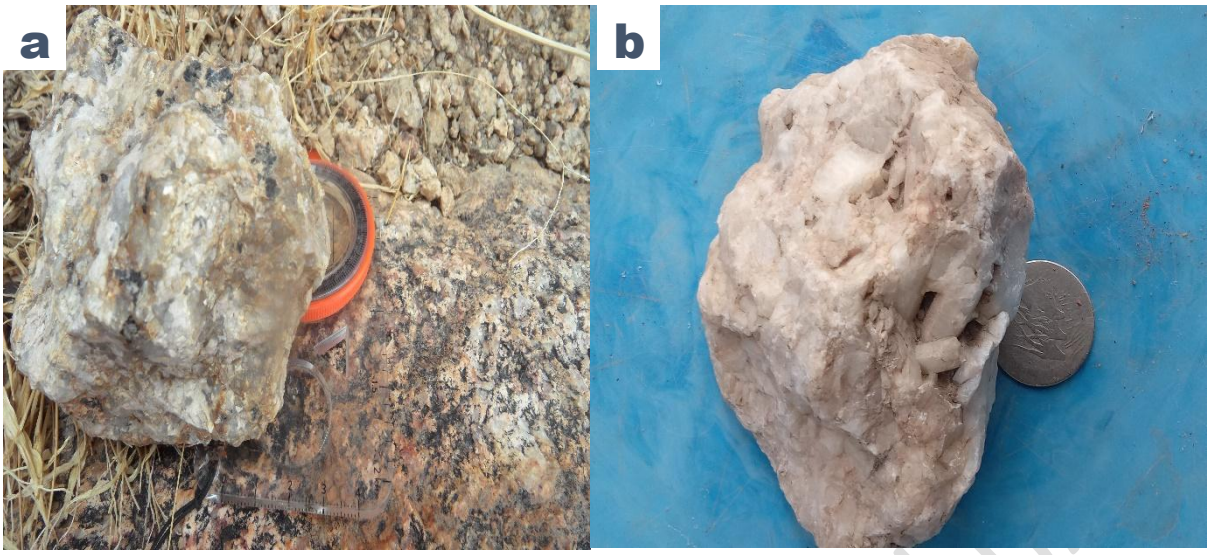

121

122

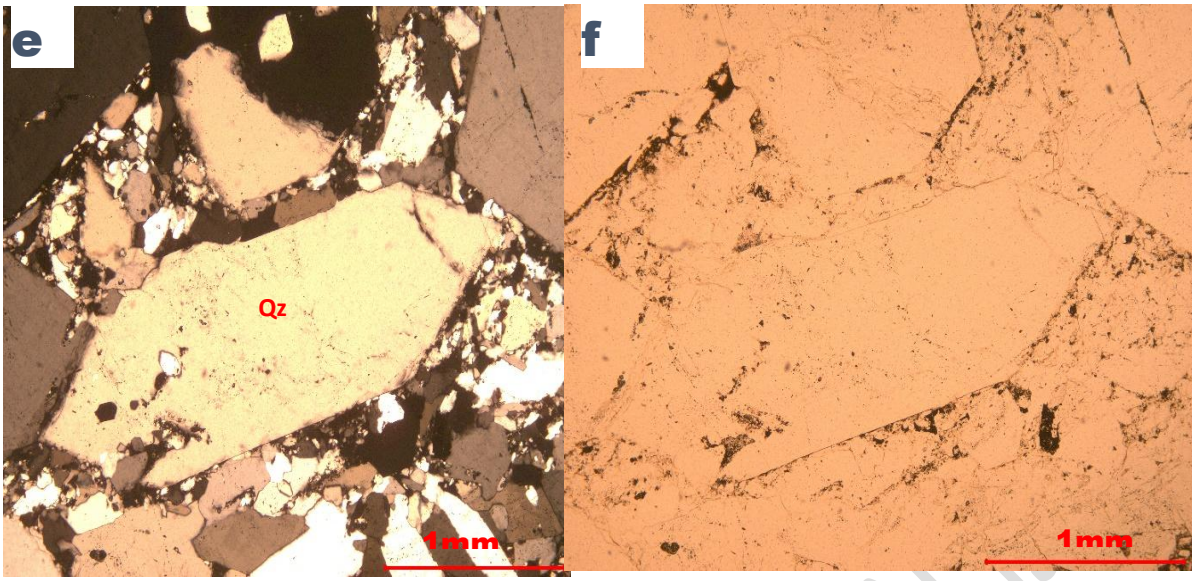

Figure 5. *Pegmatites and quartz veins of the Gleb sector. a: Outcrop of mineralized pegmatite. b: Massive milky quartz vein. c: Cataclastic texture with angular porphyroclasts (XPL). d: Anastomosing microfissures filled with iron oxides (PPL).*

3.2. Mineralogical characterization by XRD

3.2.1. Amphibole-biotite granite of Djombo (Sample DDJ)

The diffractogram of sample DDJ (Fig.6) highlights a polyphasic assemblage with a dominant crystalline nature, as evidenced by the low background noise. The major peaks are located at 20.8°, 26.6°, 27.5°, 29.4°, 40.2°, and 50.1° in 2θ, with intensities reaching ~2,900 counts.

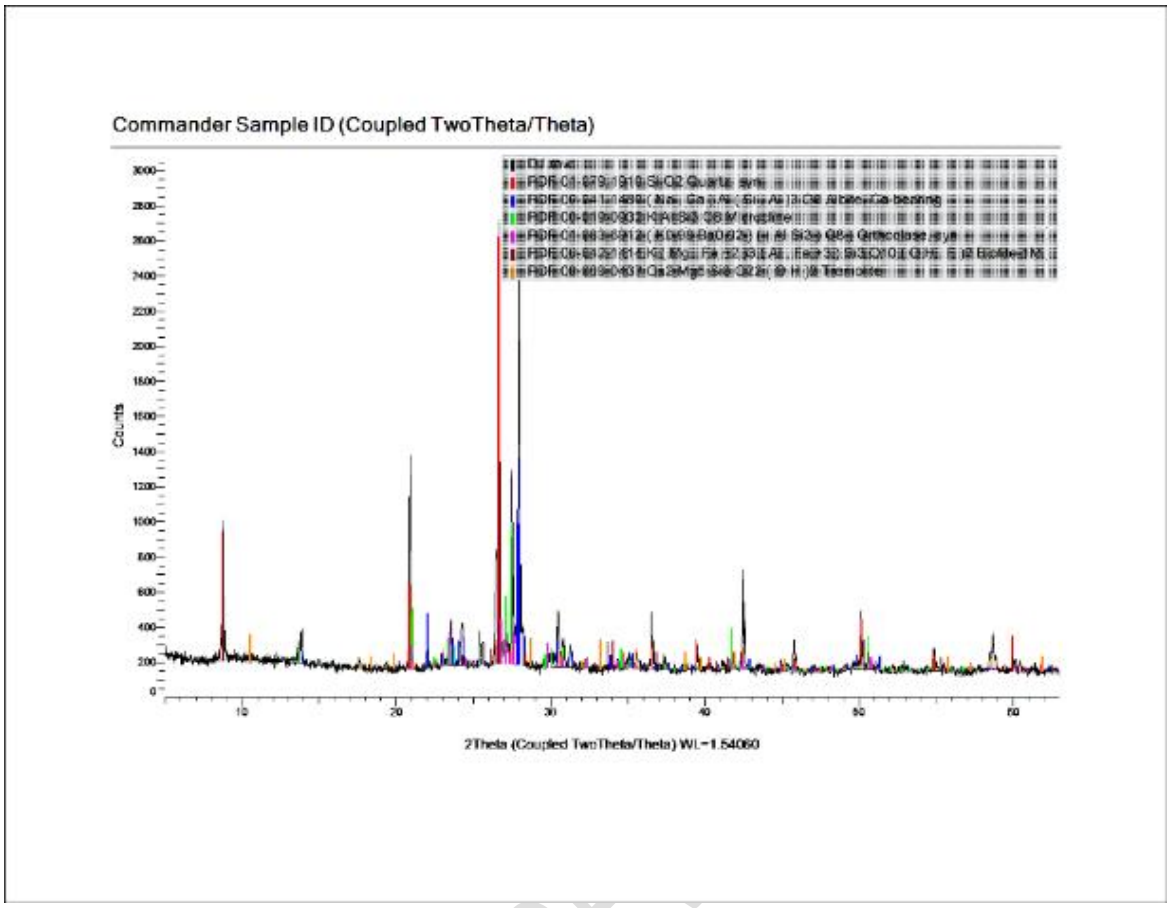

Figure 6:*X-ray diffraction (XRD) spectrum of the Djombo sample, showing reflections of quartz, albite, orthoclase, biotite, and tremolite.*

- Quartz (SiO_2): Main phase confirmed by the major peak at $2\theta \approx 26.6°$ and secondary reflections at 20.8°, 36.5°, 42.5°, and 50.1° (PDF 01-079-1910) (Fig.7).

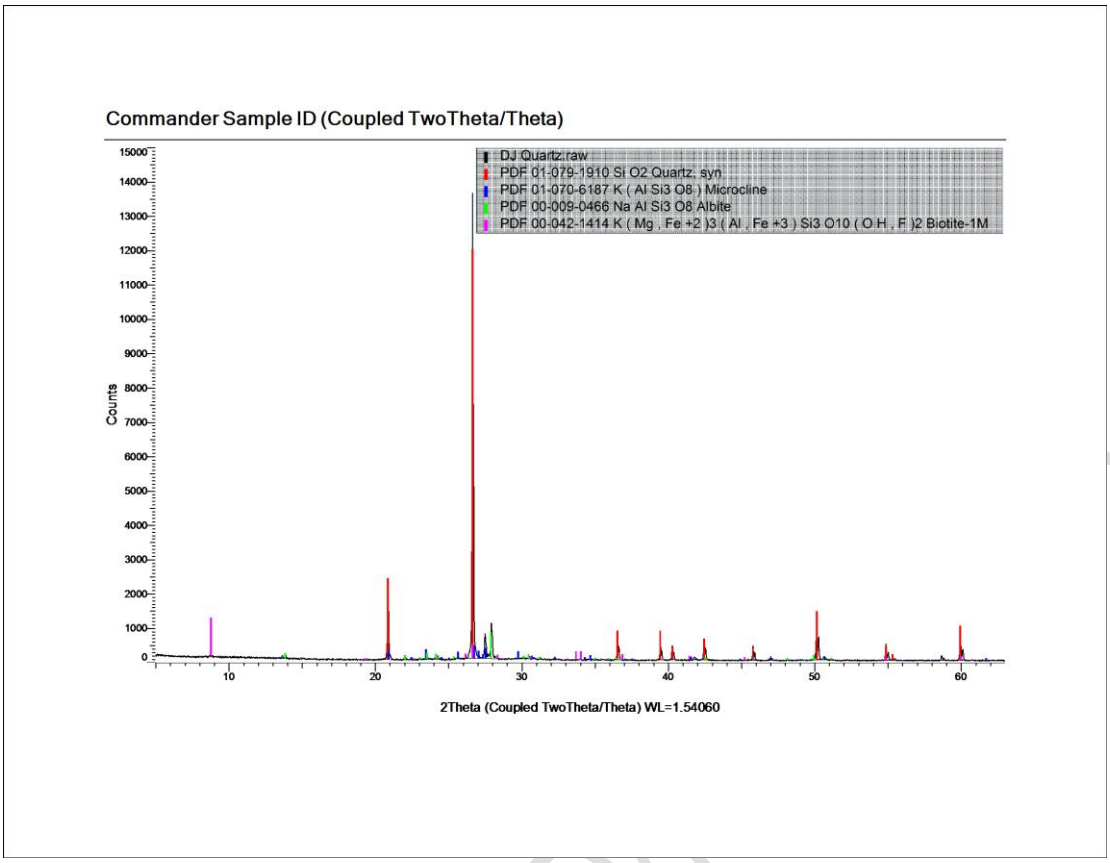

Figure 7: *XRD spectrum of the Djombo sample, showing quartz reflections.*

- Feldspars: Presence of calcic albite [$(Na,Ca)Al(Si,Al)_3O_8$] with peaks between 22-30° and 40-50° (PDF 00-041-1480), microcline ($KAlSi_3O_8$) at 20-23° and 27-30° (PDF 00-019-0932), and potentially orthoclase [$(K,Ba)(AlSi_3O_8)$] (PDF 01-083-6912) overlapping with microcline (Fig.8).

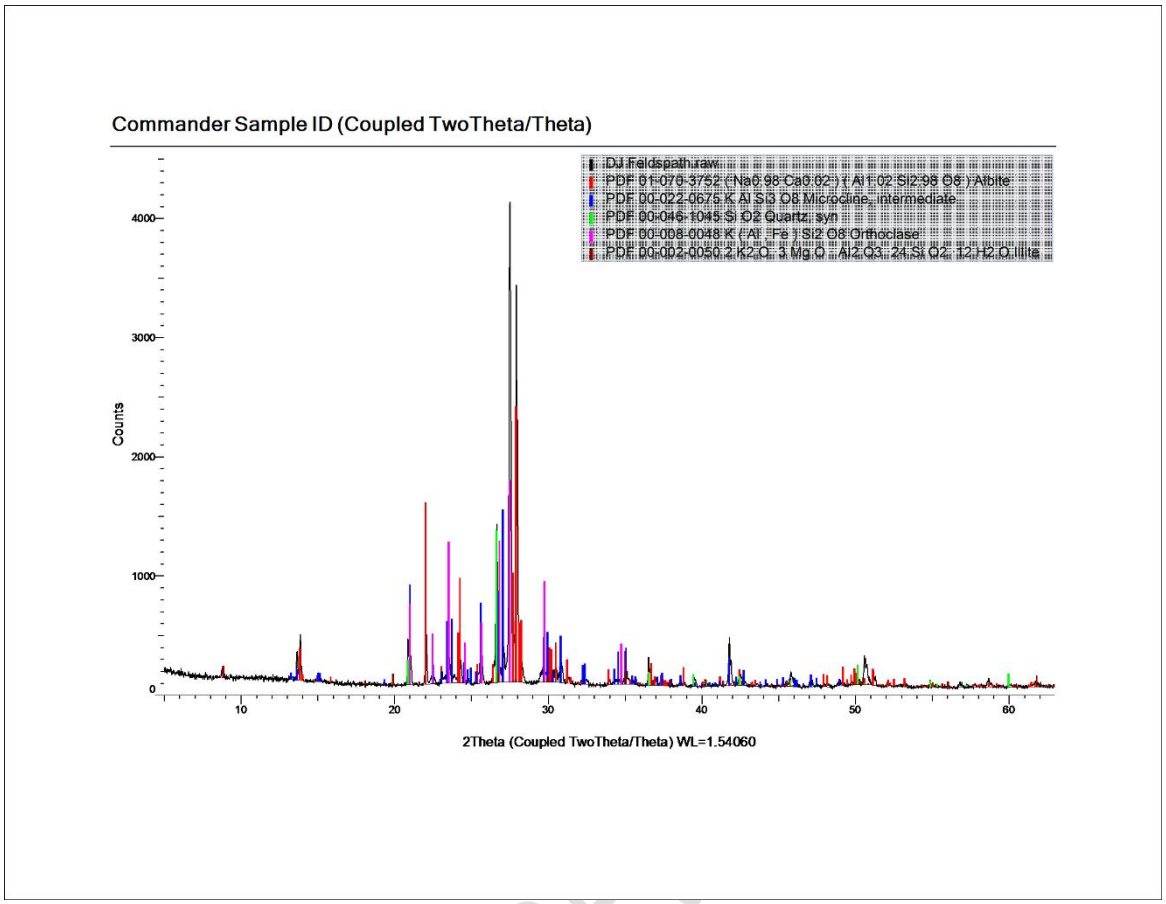

147

148 **Figure 8 :***XRD spectrum of the Djombo sample, showing feldspar reflections.*

149 - Ferromagnesian phases: Biotite-1M $[K(Mg,Fe^{2+})_3(Al,Fe^{3+})Si_3O_{10}(OH,F)_2]$ is detected by
150 low-intensity peaks around 8.5–9° (PDF 00-042-1414). Medium-intensity reflections also
151 suggest the presence of tremolite $[Ca_2Mg_5Si_8O_{22}(OH)_2]$ (PDF 00-009-0437) (Fig. 9).

152

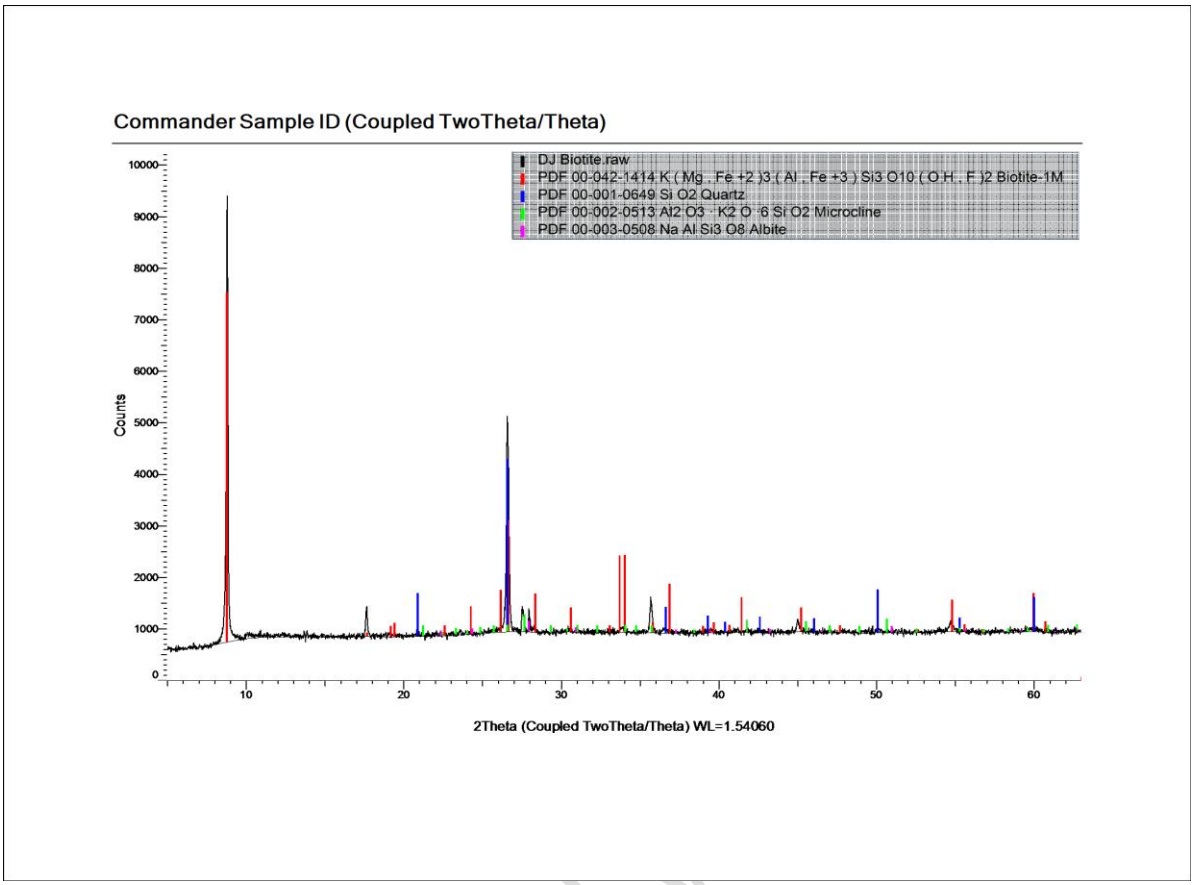

153

154 **Figure 9:***XRD spectrum of the Djombo sample, showing biotite reflections.*

155 The identified mineralogical assemblage (Table 1) is typical of a peraluminous granite having
156 undergone hydrothermal alteration under greenschist facies conditions.

157 Table 1: Mineralogical composition of the Djombo granite (DDJ)

Mineral	**Chemical formula**	**PDF reference**	**Relative abundance**
Quartz	SiO_2	01-079-1910	Dominant phase
Microcline (K-feldspar)	$KAlSi_3O_8$	00-019-0932	Second major phase
Albite (Na, Ca feldspar)	$(Na,Ca)Al(Si,Al)_3O_8$	00-041-1480	Second major phase
Biotite	$K(Mg,Fe^{2+})_3(Al,Fe^{3+})Si_3O_{10}(OH,F)_2$	00-042-1414	Subordinate phase
Trémolite	$Ca_2Mg_5Si_8O_{22}(OH)_2$	00-009-0437	Phase secondaire

3.2.2. Pegmatite of Gleb (Sample PGL I)

The diffractogram of sample PGL I (Fig.10) reveals a remarkably simple mineralogical signature, dominated by a quasi-single phase. The spectrum is characterized by intense, narrow, and well-defined peaks on an extremely low background, indicating very high crystallinity.

- α-Quartz (SiO_2): The main peak at $2\theta \approx 26.6°$ exceeds 11,000 counts, with sharp secondary reflections at 20.8°, 36.6°, 39.5°, 50.1°, and 59.9° (PDF 01-078-2315). All diagnostic quartz reflections are present and perfectly resolved.

No other mineral phase (feldspars, micas) was detected within the resolution limits of the instrument, indicating quartz of exceptional purity (>95%) and high crystallinity, typical of late hydrothermal veins.

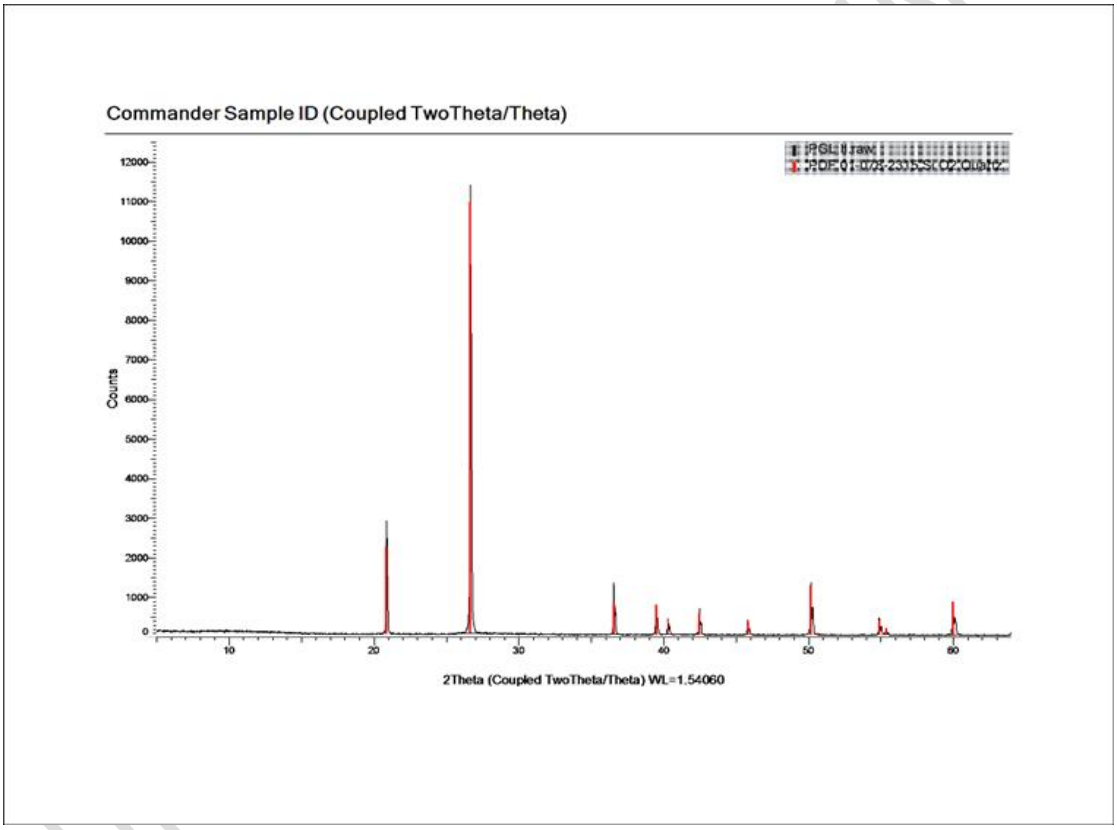

Figure 10:*XRD spectrum of the pegmatite sample, showing quartz reflections.*

4. DISCUSSION

The mineralogical assemblage of the Djombo granite (quartz-feldspars-biotite-muscovite-tremolite) reflects a peraluminous magmatism derived from crustal anatexis (Chappell and White, 1974; Barbarin, 1999), while the Gleb granite, enriched in amphibole and allanite, presents a calc-alkaline affinity typical of Pan-African post-collisional granites (Ferré et al., 2002; Penaye et al., 2006). The tremolite identified by XRD indicates hydrothermal

circulation under greenschist facies conditions (Evans, 1982), consistent with post-collisional tectonic relaxation (~570-560 Ma; Shellnutt et al., 2020; Diontar et al., 2020). This evolution fits into the model of partial destabilization of the Saharan Metacraton (Abdelsalam et al., 2002; Liégeois et al., 2013), confirmed by inherited Paleo- to Mesoproterozoic zircons (Shellnutt et al., 2017, 2020; Blades et al., 2021). The Gleb pegmatite, consisting of pure quartz (>95%) with a cataclastic texture, represents the ultimate stage of this hydrothermal evolution (Sibson et al., 1988). The association of pure quartz + cataclasis + iron oxides constitutes a classic signature of orogenic gold deposits (Groves et al., 1998; Goldfarb et al., 2005). The Haraze Djombo sector meets several favorable criteria: fertile granites enriched in rare earth elements, an active fault system, and optimal hydrothermal alteration for gold concentration (Robert and Poulsen, 2001), thereby confirming the economic potential of the Batha massif.

5. CONCLUSION

This multidisciplinary study conducted on the formations of Mounts Djombo and Gleb (Batha Massif, central Chad) has clarified their petrographic nature, mineralogical composition, and geodynamic setting within the context of the Pan-African orogeny. The host rocks are post-collisional granitoids (peraluminous biotite-muscovite granites and calc-alkaline amphibole granites) emplaced during a crustal relaxation phase (~570-560 Ma). The X-ray diffraction approach confirmed the presence of differentiated felsic assemblages (quartz, alkali feldspars, and plagioclases) modified by secondary hydrothermal alteration (tremolite). The characterization of veins and pegmatites revealed the presence of cataclastic quartz of very high crystalline purity. These structures testify to an intense circulation of late- to post-orogenic hydrothermal fluids, channeled by shear zones. This context of brittle fracturing coupled with fluid circulation confirms the strong metallogenic potential of the region, particularly for gold mineralization.

6. ACKNOWLEDGEMENTS

This work was carried out with the support of Prof. Nicolae Har, whom we thank for his hospitality at the Geology Laboratory of Babeș-Bolyai University (Cluj-Napoca, Romania) during the analytical phase, as well as the funding from the Romanian Ministry of Foreign Affairs within the framework of a mobility program organized by the AUF. We warmly thank Prof. Likius Andossa (University of N'Djamena, Chad) for proofreading this manuscript, and Prof. Rigobert Tchameni (University of Ngaoundéré, Cameroon) for his corrections and suggestions, which greatly enriched this article.

7. REFERENCES

Abdelsalam, M.G., Liégeois, J.-P., Stern, R.J., 2002. The Saharan Metacraton. Journal of African Earth Sciences 34, 119–136. https://doi.org/10.1016/S0899-5362(01)00063-4

Barbarin, B., 1999. A review of the relationships between granitoid types, their origins and their geodynamic environments. Lithos 46, 605–626. https://doi.org/10.1016/S0024-4937(98)00085-1

Blades, M.L., Shellnutt, J.G., Reavy, R.J., Jahn, B.M., 2021. Age and hafnium isotopic evolution of zircons from the Guéra Massif, south-central Chad: Implications for the evolution of the Central African Orogenic Belt. Precambrian Research 357, 106148. https://doi.org/10.1016/j.precamres.2021.106148

Braitenberg, C., Mariani, P., Ebbing, J., Sprlak, M., 2011. The enigmatic Chad lineament revisited with global gravity and gravity-gradient fields. In: The Formation and Evolution of Africa: A Synopsis of 3.8 Ga of Earth History. Geological Society, London, Special Publications 357, 329–341. https://doi.org/10.1144/SP357.18

Chappell, B.W., White, A.J.R., 1974. Two contrasting granite types. Pacific Geology 8, 173–174.

Diontar, F.M., Shellnutt, J.G., Iizuka, Y., Malservisi, R., Vishnevskaya, I.A., 2020. Mineralogy and geochemistry of the Late Ediacaran Haraze Mangueigne A-type granite (Guéra Massif, south-central Chad). Journal of African Earth Sciences 161, 103667. https://doi.org/10.1016/j.jafrearsci.2019.103667

Evans, B.W., 1982. Amphiboles in metamorphosed ultramafic rocks. Reviews in Mineralogy and Geochemistry 9B, 98–113.

Ferré, E.C., Deleris, J., Bouchez, J.L., Lar, A.U., Peucat, J.J., 2002. The Pan-African reactivation of Eburnean and Archaean provinces in Nigeria: Structural and isotopic data. Journal of the Geological Society, London 159, 83–95. https://doi.org/10.1144/0016-764901-055

Goldfarb, R.J., Baker, T., Dubé, B., Groves, D.I., Hart, C.J.R., Gosselin, P., 2005. Distribution, character, and genesis of gold deposits in metamorphic terranes. Economic Geology 100th Anniversary Volume, 407–450.

Groves, D.I., Goldfarb, R.J., Gebre-Mariam, M., Hagemann, S.G., Robert, F., 1998. Orogenic gold deposits: A proposed classification in the context of their crustal distribution and relationship to other gold deposit types. Ore Geology Reviews 13, 7–27. https://doi.org/10.1016/S0169-1368(97)00012-7

Isseini, M., Andre-Mayer, A.S., Vanderhaeghe, O., Barbey, P., Deloule, E., 2013. A-type granites from the Pan-African orogenic belt in south-western Chad constrained using geochemistry, Sr–Nd isotopes and U–Pb geochronology. Lithos 153, 39–52. https://doi.org/10.1016/j.lithos.2012.07.001

Kasser, M., 1995. Carte géologique de la République du Tchad à 1/1 500 000. BRGM, Orléans, France.

Liégeois, J.-P., Abdelsalam, M.G., Ennih, N., Ouabadi, A., 2013. Metacraton: Nature, genesis and behavior. Gondwana Research 23, 220–237. https://doi.org/10.1016/j.gr.2012.02.016

Penaye, J., Toteu, S.F., Van Schmus, W.R., Nzenti, J.P., 2006. U–Pb and Sm–Nd preliminary geochronologic data on the Yaoundé series, Cameroon: Re-interpretation of the Neoproterozoic rocks as the suture zone between the Congo craton and the Adamawa–Yadé domain. Journal of African Earth Sciences 44, 473–486. https://doi.org/10.1016/j.jafrearsci.2005.11.014

Robert, F., Poulsen, K.H., 2001. Vein formation and deformation in greenstone gold deposits. Reviews in Economic Geology 14, 111–155.

Shellnutt, J.G., Reavy, R.J., Viscaino, C., Kalsbeek, F., Jahn, B.M., 2017. The Ediacaran felsic rocks of the Guéra Massif, south-central Chad : Evidence for the northward continuation of the Neoproterozoic orogen. Precambrian Research 301, 172–190. https://doi.org/10.1016/j.precamres.2017.09.008

Shellnutt, J.G., Reavy, R.J., Yeh, M.W., Lee, T.Y., Iizuka, Y., 2020. The origin of Late Ediacaran post-collisional granites near the Chad Lineament, Saharan Metacraton, south-central Chad. Lithos 376–377, 105780. https://doi.org/10.1016/j.lithos.2020.105780

Sibson, R.H., Robert, F., Poulsen, K.H., 1988. High-angle reverse faults, fluid-pressure cycling, and mesothermal gold-quartz deposits. Geology 16, 551–555.

Sobh, M., Ebbing, J., Mansi, A.H., Götze, H.J., 2020. Inverse and 3D forward gravity modelling for the estimation of the crustal thickness of Egypt. Tectonophysics 752, 52–68. https://doi.org/10.1016/j.tecto.2018.12.002

Vincent, P.M., 1956. Carte géologique de reconnaissance du Tchad (feuilles de Mongo, Melfi, Abou Déïa, Am Timan). Gouvernement Général de l'A.E.F., Service des Mines, Brazzaville.